J|A|C|S ARTICLES

Published on Web 07/01/2009

# Templating Molecular Arrays in Amyloid's Cross-$\beta$ Grooves

W. Seth Childers, Anil K. Mehta, Kun Lu, and David G. Lynn*

*Center for Fundamental and Applied Molecular Evolution (FAME), and Department of Chemistry and Biology, Emory University, Atlanta, Georgia 30322*

Received March 24, 2009; E-mail: david.lynn@emory.edu

***Abstract:*** Amyloid fibers, independent of primary amino acid sequence, share a common cross-$\beta$ structure and bind the histochemical dye Congo Red (CR). Despite extensive use of CR in amyloid diagnostics, remarkably little is known about the specific and characteristic binding interactions. Fibril insolubility, morphological inhomogeneity, and multiple possible ligand binding sites all conspire to limit characterization. Here, we have exploited the structure of cross-$\beta$ nanotubes, which limit the number of potential binding sites, to directly interrogate cross-$\beta$ laminate grooves. CR bound to cross-$\beta$ nanotubes displays the hallmark apple-green interference color, a broad red-shifted low energy transition, and a $K_d$ of $1.9 \pm 0.5$ $\mu$M. Oriented electron diffraction and linear dichroism defines the orientation of CR as parallel to the amyloid long axis and colinear with laminate grooves. The broad red-shifted UV signature of CR bound to amyloid can be explained by semiempirical quantum calculations that support the existence of a precise network of J- and H-CR aggregates, illuminating the ability of the amyloid to organize molecules into extended arrays that underlie the remarkable diagnostic potential of CR.

## Introduction

For more than 80 years, Congo Red (CR) has served as a seemingly universal diagnostic of amyloid structure.[1] When CR stained amyloid is viewed under crossed polarized light, a characteristic "apple-green birefringence", more appropriately termed apple-green interference color,[2,3] provides a signature for amyloid, even in heterogeneous plaque deposits. Remarkably, CR can identify amyloid cross-$\beta$ structure of polypeptides with drastically different primary sequences and lengths ranging from neurodegenerative disease amyloid,[4] misfolded globular proteins,[5] functional amyloid,[6−8] and synthetic truncated cross-$\beta$ structures.[9,10] Additionally, CR binding is invariant to parallel[4] or antiparallel $\beta$-sheet registry within amyloid cross-$\beta$ structure.[11,12] From the bends and disordered regions in A$\beta$(1−40)[13,14] to the triangular beta solenoid in HET-s(218−289),[15] the surface variation expected to exist across the known amyloid structures is immense. Paradoxically, spectroscopic signatures of CR binding are remarkably similar (a broad red-shifted UV−vis transition[4,16]), suggesting the existence of a common CR binding mode, and the relationship between CR binding and amyloid structure[17] remains unclear despite extensive investigation.[18,19]

Biophysical characterization via solid-state NMR,[20,21] fiber diffraction,[22,23] and crystallography on amyloid microcrystals[24] has resulted in well-defined structural models for the cross-$\beta$ spine of amyloid. Oriented diffraction patterns of all amyloids reveal the characteristic cross-$\beta$ pattern.[22,25] Orthogonal reflections at 4.7 and ~10 Å are assigned to H-bonded peptides, with the peptide backbone oriented perpendicular to fiber axis, and

(1) Divry, P. F. M. *Omptes rendus des seances de la societie de biologie et de ses filiales* **1927**, *97*, 1808.
(2) Howie, A. J.; Brewer, D. B. *Micron* **2009**, *40*, 285.
(3) Kaminksy, W.; Jin, L. W.; Powell, S.; Maezawa, I.; Claborn, K.; Branham, C.; Kahr, B. *Micron* **2006**, *37*, 324.
(4) Klunk, W. E.; Jacob, R. F.; Mason, R. P.; Ronald, W. *Methods in Enzymology*; Academic Press: New York, 1999; Vol. 309, p 285.
(5) Guijarro, J. I. a.; Sunde, M.; Jones, J. A.; Campbell, I. D.; Dobson, C. M. *Proc. Natl. Acad. Sci. U.S.A.* **1998**, *95*, 4224.
(6) Glover, J. R.; Kowal, A. S.; Schirmer, E. C.; Patino, M. M.; Liu, J.-J.; Lindquist, S. *Cell* **1997**, *89*, 811.
(7) Iconomidou, V. A.; Vriend, G.; Hamodrakas, S. J. *FEBS Lett.* **2000**, *479*, 141.
(8) Fowler, D. M.; Koulov, A. V.; Alory-Jost, C.; Marks, M. S.; Balch, W. E.; Kelly, J. W. *PLoS Biol.* **2006**, *4*, e6.
(9) Inouye, H.; Nguyen, J. T.; Fraser, P. E.; Shinchuk, L. M.; Packard, A. B.; Kirschner, D. A. *Amyloid* **2000**, *7*, 179.
(10) Tenidis, K.; Waldner, M.; Bernhagen, J. R.; Fischle, W.; Bergmann, M.; Weber, M.; Merkle, M.-L.; Voelter, W.; Brunner, H.; Kapurniotu, A. *J. Mol. Biol.* **2000**, *295*, 1055.
(11) Van Nostrand, W. E.; Melchor, J. P.; Cho, H. S.; Greenberg, S. M.; Rebeck, G. W. *J. Biol. Chem.* **2001**, *276*, 32860.
(12) Tycko, R.; Sciarretta, K. L.; Orgel, J. P. R. O.; Meredith, S. C. *Biochemistry*, DOI: 10.1021/bi9002666.
(13) Petkova, A. T.; Ishii, Y.; Balbach, J. J.; Antzutkin, O. N.; Leapman, R. D.; Delaglio, F.; Tycko, R. *Proc. Natl. Acad. Sci. U.S.A.* **2002**, *99*, 16742.
(14) Petkova, A. T.; Yau, W. M.; Tycko, R. *Biochemistry* **2006**, *45*, 498.
(15) Wasmer, C.; Lange, A.; Van Melckebeke, H.; Siemer, A. B.; Riek, R.; Meier, B. H. *Science* **2008**, *319*, 1523.
(16) Klunk, W. E.; Pettegrew, J. W.; Abraham, D. J. *J. Histochem. Cytochem.* **1989**, *37*, 1273.
(17) Puchtler, H.; Sweat, F.; Levine, M. *J. Histochem. Cytochem.* **1962**, *10*, 355.
(18) Frid, P.; Anisimov, S. V.; Popovic, N. *Brain Res. Rev.* **2007**, *53*, 135.
(19) Kurimoto, M.; Müller, B.; Kaminsky, W.; Kahr, B.; Jin, L.-W. *Mol. Cryst. Liq. Cryst.* **2002**, *389*, 1.
(20) Benzinger, T. L.; Gregory, D. M.; Burkoth, T. S.; Miller-Auer, H.; Lynn, D. G.; Botto, R. E.; Meredith, S. C. *Proc. Natl. Acad. Sci. U.S.A.* **1998**, *95*, 13407.
(21) Petkova, A. T.; Ishii, Y.; Balbach, J. J.; Antzutkin, O. N.; Leapman, R. D.; Delaglio, F.; Tycko, R. *Proc. Natl. Acad. Sci. U.S.A.* **2002**, *99*, 16742.
(22) Eanes, E. D.; Glenner, G. G. *J. Histochem. Cytochem.* **1968**, *16*, 673.
(23) Serpell, L. C.; Smith, J. M. *J. Mol. Biol.* **2000**, *299*, 225.
(24) Sawaya, M. R.; Sambashivan, S.; Nelson, R.; Ivanova, M. I.; Sievers, S. A.; Apostol, M. I.; Thompson, M. J.; Balbirnie, M.; Wiltzius, J. J. W.; McFarlane, H. T.; Madsen, A. O.; Riekel, C.; Eisenberg, D. *Nature* **2007**, *447*, 453.

  

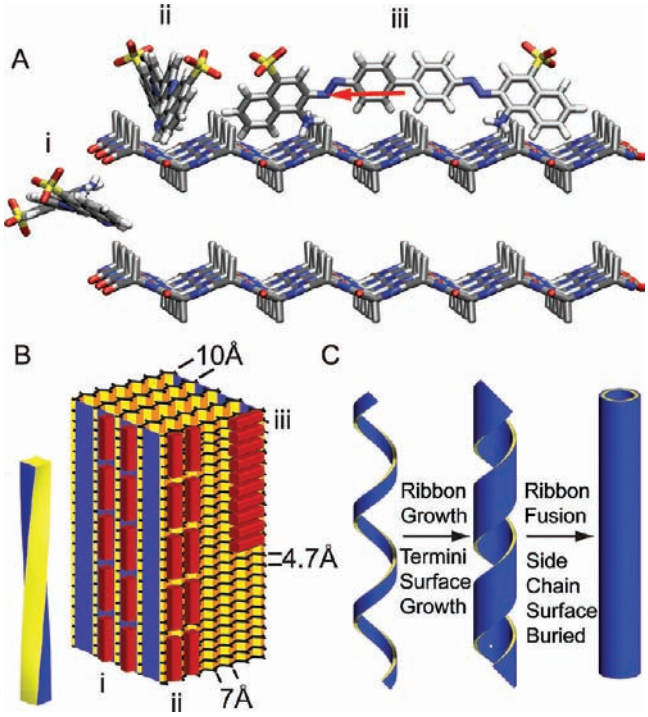


***Figure 1.*** Proposed binding modes for CR. (A) The amyloid cross-$\beta$ structure contains three possible sites: (i) laminate groove, (ii) pleat groove, and (iii) between two peptides. The calculated transition dipole is shown as a red arrow across binding mode iii. (B) The amyloid fiber has two distinct solvent-exposed surfaces: one composed of side-chains (yellow) and one composed of N−C termini (blue). On the termini surfaces (blue), CR (red) binds in a single mode within laminate grooves in which molecules are organized end-to-end. On the side-chain surface (yellow), two binding modes are available: between $\beta$-sheet pleats that organize CR end-to-end and between peptide $\beta$-strands, which organize CR molecules side-by-side and perpendicular to fiber long-axis. (C) Transformation from amyloid fiber to nanotube. An increase in the number of laminates increases the N−C termini surface area (blue). Fusion into a tube blocks the side-chain surface (yellow) except at the very ends of the nanotube.

to the $\beta$-sheet lamination direction, respectively (Figure 1). In its simplified form, amyloid's solvent-exposed surfaces can be approximated as a twisted rectangular rod (Figure 1A and B) with two pairs of like faces: one lined with side-chains emerging from the $\beta$-sheet pleats (Figure 1B, yellow) and the other exposing the N- and C-terminal residues of the $\beta$-sheet laminates (Figure 1B, blue). From this model, the yellow surface has two possible CR binding orientations: (a) between the H-bonded strands where the peptides are separated by 4.7 Å,[26,27] placing CR perpendicular to the fiber long-axis (Figure 1A, iii), and (b) within the $\beta$-sheet pleats, packed between side-chains of the i and i+2 residues and parallel to the fiber long-axis (Figure 1A, ii). In contrast, the blue surface presents $\beta$-sheets separated by ~10 Å and laminate grooves where CR could bind along the long fiber axis[16,28] (Figure 1A, i). Additionally, the fiber ends present binding sites, but these are at low stoichiometry relative to the other surfaces. This complex dimensionality of the amyloid fiber has presented a major hurdle for the identification of ligand binding sites[29,30] and complicated the design of both diagnostic and therapeutic agents.

To reduce the dimensionality of amyloid assemblies, we have focused on the nucleating center of the A$\beta$ peptide of Alzheimer's disease. $^{16}$KLVFFA$^{22}$E or A$\beta$(16−22) is essential for amyloid nucleation,[31] and mutations within the region modulate A$\beta$ toxicity.[32] A$\beta$(16−22) forms both classical cross-$\beta$ amyloid fibers[33,34] and helical cross-$\beta$ nanotubes[34−36] with antiparallel $\beta$-sheets. This reduces the complexity of the peptide termini surfaces (blue in Figure 1B,C) to a single type relative to parallel $\beta$-sheet assemblies,[37] which contain unique N-terminal and C-terminal surfaces. In the nanotubes, a shift in $\beta$-sheet registry results in an increase in the number of $\beta$-sheet laminates[34,36,38] from 5 in the fibers to more than 100. When the edges of the resulting helical ribbons fuse (Figure 1C), the amino acid side-chain surfaces (yellow) are completely buried upon tube formation. The nanotube's only solvent-exposed surface (blue) is the cross-$\beta$ laminate grooves (Figure 1A, i), allowing CR's affinity to be interrogated directly at this surface.

## Materials and Methods

**Peptide Synthesis and Purification.** Peptides were synthesized using standard FMOC NMM/HBTU protocols for solid-phase synthesis and capped at the N- and C-termini with $CH_3CO-$ and $-NH_2$, respectively. Peptides were purified via RP-HPLC using C18-reverse phase with an acetonitrile−water gradient. MALDI-TOF with a 2,5-dihydroxybenzoic acid matrix confirmed molecular weight. A$\beta$(16−22)E22L (1.3 mM) dissolved in 40% $CH_3CN/H_2O$ with 0.1% TFA (pH 2) was assembled at 4 °C until mature by CD, ~2 weeks.[34] Assemblies were titrated to pH 7 using 0.1 M NaOH in 40% $CH_3CN$.

**Transmission Electron Microscopy and Electron Diffraction.** TEM micrographs were recorded with a Philips 410 TEM with a Tungsten filament at an accelerating voltage of 80 kV. Upon addition to TEM grids, the KLVFFAL assemblies were allowed to adsorb for 1 min. Excess peptide solution was wicked away with filter paper. The 2 wt % uranyl acetate incubation time was optimized for negative staining both inside and outside of the hollow nanotubes. The micrographs were recorded at magnifications between 7100× and 69 000×. Negatives were scanned at 2000 dpi resolution on an Agfa DuoScan flatbed scanner (Agfa Corp., Ridgefield Park, NJ), and $d$-spacing was calculated using $d = \lambda L/R$, where $R$ is the distance (mm) from the central bright spot to one of the rings, $L$ (mm) is the distance between specimen and photographic film, and $\lambda$ is the electron wavelength (80 kV). Camera length was calibrated using an aluminum polycrystalline standard (Ted Pella, Inc., Redding, CA). Given the shorter $d$-spacings for evaporated aluminum relative to the amyloid nanotubes, an additional standard with $d$-spacings comparable to KLVFFAL nano-

(25) Geddes, A. J.; Parker, K. D.; Atkins, E. D. T.; Beighton, E. *J. Mol. Biol.* **1968**, *32*, 343.
(26) Turnell, *J. Mol. Biol.* **1992**, *227*, 1205.
(27) Carter, D. B.; Chou, K. C. *Neurobiol. Aging* **1998**, *19*, 37.
(28) William, E. K.; Manik, L. D.; Jay, W. P. *Neurobiol. Aging* **1995**, *16*, 541.
(29) Levine, I. I. I. H. *Amyloid* **2005**, *12*, 5.
(30) Wu, C.; Wang, Z.; Lei, H.; Zhang, W.; Duan, Y. *J. Am. Chem. Soc.* **2007**, *129*, 1225.
(31) Wurth, C.; Guimard, N. K.; Hecht, M. H. *J. Mol. Biol.* **2002**, *319*, 1279.
(32) Melchor, J. P.; McVoy, L.; Van Nostrand, W. E. *J. Neurochem.* **2000**, *74*, 2209.
(33) Balbach, J. J.; Ishii, Y.; Antzutkin, O. N.; Leapman, R. D.; Rizzo, N. W.; Dyda, F.; Reed, J.; Tycko, R. *Biochemistry* **2000**, *39*, 13748.
(34) Mehta, A. K.; Lu, K.; Childers, W. S.; Liang, Y.; Dublin, S. N.; Dong, J.; Snyder, J. P.; Pingali, S. V.; Thiyagarajan, P.; Lynn, D. G. *J. Am. Chem. Soc.* **2008**, *130*, 9829.
(35) Lu, K.; Jacob, J.; Thiyagarajan, P.; Conticello, V. P.; Lynn, D. G. *J. Am. Chem. Soc.* **2003**, *125*, 6391.
(36) Liang, Y.; Pingali, S. V.; Jogalekar, A. S.; Snyder, J. P.; Thiyagarajan, P.; Lynn, D. G. *Biochemistry* **2008**, *47*, 10018.
(37) Nelson, R.; Sawaya, M. R.; Balbirnie, M.; Madsen, A. O.; Riekel, C.; Grothe, R.; Eisenberg, D. *Nature* **2005**, *435*, 773.
(38) Dong, J.; Lu, K.; Lakdawala, A.; Mehta, A. K.; Lynn, D. G. *Amyloid* **2006**, *13*, 206.

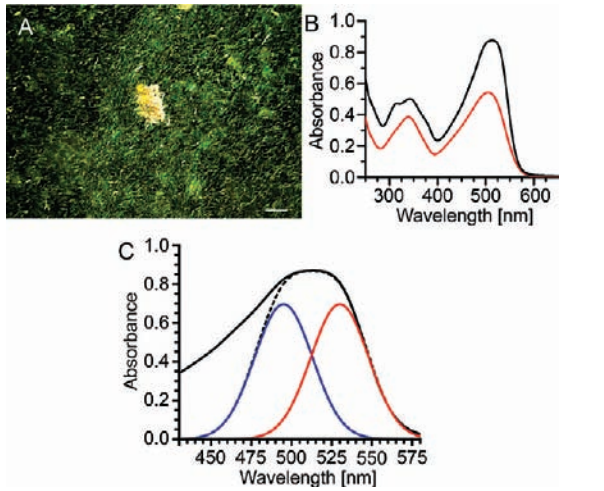


***Figure 2.*** Interaction of CR with KLVFFAL amyloid nanotubes. (A) Images of nanotubes assembled from 1.3 mM KLVFFAL in 40% acetonitrile at pH 7, then bundled using 18 mM $Na_2SO_4$ and stained with 100 $\mu$M CR viewed between crossed polarizers. (B) UV−vis spectra of 65 $\mu$M CR (black line) and KLVFFAL nanotubes (formed from 650 $\mu$M peptide) + 65 $\mu$M CR (red line). (C) Gaussian fits of CR bound transition with a 10 nm blue-shift and 25 nm red-shift.

tubes was required. A$\beta$(16−22) nanotubes with *d*-spacings of 4.7 and 9.9 Å, confirmed by fiber X-ray diffraction, were employed as a standard.[34]

**UV−Vis Absorption and Circular Dichroism.** UV−vis absorption spectra were recorded with a Jasco V-530 UV spectrophotometer using a 2 mm cuvette path length. Dissolving CR in 40% acetonitrile at pH 6 shifted the $\lambda_{max}$ from 498 to 505 nm. CR molar absorptivity at 505 nm was determined to be 39 239 L mol$^{-1}$ cm$^{-1}$ in 40% acetonitrile at pH 7 and was found to be insensitive from pH 6−8. Both UV and CD spectra were background subtracted using KLVFFAL nanotubes in the absence of CR to minimize scattering effects. CD spectra were measured on a Jasco V-810 CD polarimeter with a 1 mm cuvette. Plots of $\lambda_{max}$ in Figure 7B and D represent the average $\lambda_{max}$ for three independent trials; the error bar represents wavelengths whose absorbance is within 95% of $\lambda_{max}$.

**Hill Plot.** Molar absorptivity at 532 nm was 56 604 L mol$^{-1}$ cm$^{-1}$ for bound CR under conditions with excess nanotubes, while the molar absorptivity for free CR was 39 239 L mol$^{-1}$ cm$^{-1}$. After correction for scattering, a clear isosbestic point was identified at 406 nm with a molar absorptivity of 15 195 L mol$^{-1}$ cm$^{-1}$ as shown in Figure 2. The moles of bound CR were calculated following protocols[4] established for CR UV−vis absorption spectral assays[4] (see Figure 2C). The amount of bound CR was calculated as ($A_{532}$/39 239 − $A_{406}$/15 195)/((56 604/39 239) − 1) for each saturation point in Figure 3. $\theta$ in Figure 3B is the fraction of occupied binding sites (CR bound)/(total CR), where total CR binding was determined from the maximum in Figure 3B. Error bars in Figure 3 represent the standard deviation of three independent trials, and each trial is the average of three scans.

**Linear Dichroism.** This was recorded using a microvolume cuvette with a path length of 50 $\mu$m[39] and a rotation speed of 3000 rpm to establish Couette flow. The background scattering for each sample was obtained from the LD spectra of samples at 0 rpm. From Figure 5B, LD of bound CR was determined to be 0.060, with corresponding isotropic UV of 0.096. For the bound CR complex, $LD^R$ was determined to be 0.62. If *S* is equivalent to 1, then $\alpha = 14°$, and when $S = 0.8$, $\alpha = 0°$. For additional details regarding the calculations, see the Supporting Information Materials and Methods.

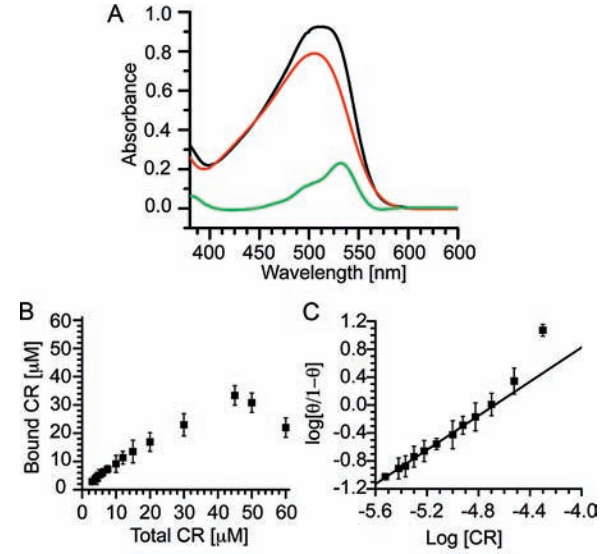


***Figure 3.*** (A) UV−vis absorbance comparison of 10 $\mu$M CR (red), 10 $\mu$M CR + 200 $\mu$M KLVFFAL (black) background corrected, and difference (green). (B) Concentration of bound CR. The binding of CR to 200 $\mu$M assembled nanotubes was determined by the electronic transitions at 532 and 406 nm. Maximum binding occurred at 33.4 $\mu$M. (C) Hill plot analysis of CR saturation binding gave a slope of 1.2 ± 0.2 and *y*-intercept of 5.71.

**Polarizing Microscopy.** KLVFFAL nanotubes have a diameter of 38 nm[34] and are below the resolution of optical microscopy (~200 nm). We have previously reported that positively charged nanotubes can be bundled by addition of divalent anions (e.g., sulfate) and create lamellar arrays of nanotubes that are large enough to be visualized.[40] Following published methods,[41] the sulfate bundled nanotubes[40] were stained with CR. The sulfate bundled peptide nanotube solution (3 $\mu$L) was air-dried on a glass microscope slide, and the CR staining solution (100 $\mu$L) was added and allowed to air-dry. The slide was then washed with double distilled $H_2O$ to remove unbound CR and again allowed to air-dry. Optical microscopy images were measured with an Olympus BX60 differential interference contrast microscope under crossed polarizers at a magnification of 40×. Bright field images were obtained by tuning the angle between polarizers to 0°.

**Quantum Calculations.** All calculations were performed with Gaussian 03.[42] The DFT 6-31+G(d,p)/B3LYP geometry optimized Congo Red monomer was fixed when creating the dimers, trimers, and tetramers. ZINDO/S[43,44] calculations of vertical electronic transitions were limited by memory requirements to a maximum of 4 CR molecules. Exciton coupling is the difference (i.e., energy shift) between the calculated vertical transition energies for the multimers and monomer. Simulated UV spectra in Figure 9 are a sum of Gaussians with a 20 nm full width half-maximum (fwhm) weighted by the calculated oscillator strength for all transitions (Figure S1). Spectra in Figure 9 are from calculations of the H-aggregate ($r$ = 10.2 Å) tetramer, J-aggregate ($r$ = 28.2 Å) tetramer, and the trimer/monomer in Figure 8D with $r$ = 14.1 Å.

## Results

**CR Binds to KLVFFAL Nanotubes.** Unlike most amyloids, A$\beta$(16−22) assemblies remain soluble,[34] avoiding scattering

(39) Marrington, R.; Dafforn, T. R.; Halsall, D. J.; MacDonald, J. I.; Hicks, M.; Rodger, A. *The Analyst* **2005**, *130*, 1608.
(40) Lu, K.; Guo, L.; Mehta, A. K.; Childers, W. S.; Dublin, S. N.; Skanthakumar, S.; Conticello, V. P.; Thiyagarajan, P.; Apkarian, R. P.; Lynn, D. G. *Chem. Commun.* **2007**, 2729.
(41) Nilsson, M. R. *Methods* **2004**, *34*, 151.
(42) Frisch, M. J.; Schledgel, H. B.; Scuseria, G. E.; Robb, M. A.; Cheeseman, J. R.; Montgomery, J. A.; Vreven, K. N. *Gaussian 03*; Gaussian, Inc.: Wallingford, CT, 2004.
(43) Bacon, A. D.; Zerner, M. C. *Theor. Chim. Acta* **1979**, *53*, 21.
(44) Thompson, M. A.; Zerner, M. C. *J. Am. Chem. Soc.* **1991**, *113*, 8210.

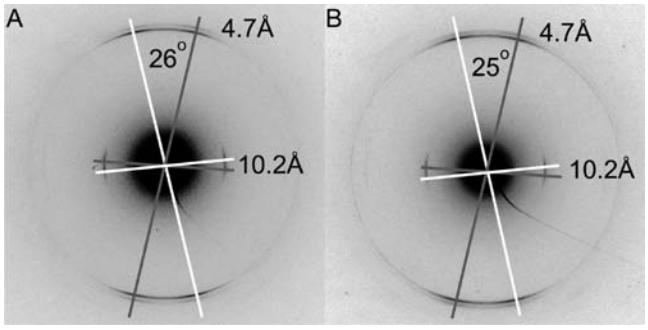


***Figure 4.*** Electron diffraction of (A) KLVFFAL amyloid nanotubes and (B) KLVFFAL amyloid nanotubes (650 $\mu$M peptide) + 65 $\mu$M CR. Diffraction of tubes oriented vertically in this presentation reveals two cross-$\beta$ patterns composed of 4.7 and 10.2 Å distances as illustrated by the gray and white crosses. The offset between hydrogen-bonding arcs of each cross-$\beta$ pattern is 26° ± 2° without and 25° ± 2° with CR, respectively.

complications commonly observed with protein aggregates.[4,16] Under neutral conditions, A$\beta$(16−22)E22L, KLVFFAL, also self-assembles as soluble hollow nanotubes with homogeneous diameters.[34] With the addition of CR, the typical transition at 505 nm in 40% acetonitrile[45] red-shifts to 515 nm, and the molar absorptivity increases by nearly 50% (Figure 2B). The broad transition is consistent with CR binding to amyloid,[4,16] but, in this case, can be fit to two Gaussians with $\lambda_{max}$ of 495 nm (10 nm blue-shift) and 530 nm (25 nm red-shift).

In the presence of $Na_2SO_4$, KLVFFAL nanotubes assemble into supramacromolecular filamentous bundles of nanotubes easily visualized by optical microscopy.[40] CR appears to accumulate along the surface of these supramacromolecular assemblies, and, when viewed through crossed polarizers, displays the characteristic apple-green interference color (Figure 2A) of amyloid assemblies.[1]

For Hill plot analysis, the KLVFFAL nanotube concentration was reduced from 650 to 200 $\mu$M to reduce potential scattering effects. A representative comparison of 10 $\mu$M CR + 200 $\mu$M KLVFFAL nanotubes, 10 $\mu$M CR, and the difference are shown in Figure 3A. This figure contains the isosbestic point assignment at 406 nm and a maximal difference between free and bound CR at 532 nm. A broad and representative selection of fully corrected spectra is shown in Supporting Information Figure S3. The CR spectral shift assay was used to estimate the bound concentration[4] (Figure 3B), and at saturation, the KLVFFAL:CR binding ratio was 6.1 ± 0.5. Binding cooperativity (Figure 3C) evaluation gave a Hill coefficient of 1.2 ± 0.2 and $K_d$ of 1.9 ± 0.5 $\mu$M, consistent with noncooperative CR binding to a single site along the solvent-exposed laminate grooves. However, at high CR concentrations, deviation from linearity was observed and could be attributed to increased light scattering, a change in bound CR molar absorptivity, or even binding of an additional CR within the laminate groove.

**CR Binding Does Not Alter Cross-$\beta$ Structure.** TEM micrographs show no significant changes in KLVFFAL nanotube morphology when saturated with CR (Figure S2). Electron diffraction micrographs of oriented nanotubes (Figure 4) are also unaltered by CR binding and display two clear cross-$\beta$ patterns, each assigned to H-bonded peptides at 4.7 Å and perpendicular $\beta$-sheet laminates (sheet-stacking) at 10.2 Å. The double pattern arises from flattened top and bottom walls of the tubes following drying on the TEM grid.[34] In both cases, the two cross-$\beta$ patterns are tilted by 13 ± 2° from the nanotube long-axis. If CR molecules intercalate into the cross-$\beta$ structure,[26,27] they do so without distortions of the repeating laminating arrays.

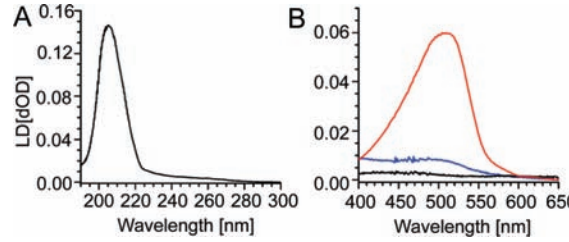


***Figure 5.*** Couette flow LD of KLVFFAL amyloid nanotubes. Panels show (A) the nanotube amide transition and (B) 650 $\mu$M CR with (red) and without (blue) 650 $\mu$M nanotubes. The positive LD indicates that both electronic transition dipoles are oriented parallel to direction of flow.

**CR Is Oriented Along the Nanotube Surface.** Linear dichroism (LD), measured with a Couette flow cell[46] that orients the KLVFFAL cross-$\beta$ nanotubes, was used to evaluate the orientation of CR with respect to the nanotube axis. The electronic transition dipole of the 200 nm amide $\pi-\pi^*$ transition lies along the C═O bond[47,48] collinear with the H-bonds in a $\beta$-sheet and gives a positive LD signature (Figure 5A). This positive LD indicates the amide absorption is greater parallel than perpendicular to the tube axis and orients the backbone carbonyl roughly parallel to the tube long axis.

KLVFFAL nanotubes have no electronic transitions between 400 and 650 nm, and CR by itself displays only a weak positive LD signature, consistent with laminar flow orienting a small percentage of the linear CR molecules (Figure 5B).[47] In contrast, the LD of CR bound to KLVFFAL nanotubes (Figure 5B) displays a strong positive signature at 515 nm, indicating preferred absorbance parallel to the tube axis. As the transition dipole of CR for this low-energy transition is parallel to the molecular long axis (Figure 1A),[19] CR is oriented roughly parallel to the tube axis. The calculated orientation factor ($S$) is between 0.8 and 1.0, allowing placement of the CR transition dipole within 0−14° of the nanotube axis which is within the 13 ± 2° offset of the laminate grooves of the KLVFFAL amyloid tubes.

**CR Docking Model.** Atomic-level amyloid models were created using electron diffraction $d$-spacing and specific $^{13}C-^{15}N$ interstrand distances obtained with solid-state NMR.[34] No structural restraints were applied during the molecular dynamics (MD) search for local energy minima, and all models consistent with electron diffraction H-bonding (4.7 Å) and lamination $d$-spacing (10.2 Å) were retained. The resulting model in Figure 6 shows two laminated $\beta$-sheets, each composed of 6 H-bonded peptides, together forming a solvent-accessible laminate groove.

The functional groups that line the laminate groove are composed of N-terminal acetate (cyan), lysine-16 (blue), leucine-17 (orange), leucine-22 (yellow), and the C-amide (brown). These functional groups form an amphiphilic surface composed of hydrophobic as well as charged lysine side-chains. CR

(45) Pigorsch, E.; Elhaddaoui, A.; Turrell, S. *Spectrochim. Acta, Part A: Mol. Biomol. Spectrosc.* **1994**, *50*, 2145.
(46) Marrington, R.; Dafforn, T. R.; Halsall, D. J.; Rodger, A. *Biophys. J.* **2004**, *87*, 2002.
(47) Rodger, A.; Marrington, R.; Geeves, M. A.; Hicks, M.; Alwis, L. d.; Halsall, D. J.; Dafforn, T. R. *Phys. Chem. Chem. Phys.* **2006**, *8*, 3161.
(48) Dafforn, T. R.; Rajendra, J.; Halsall, D. J.; Serpell, L. C.; Rodger, A. *Biophys. J.* **2004**, *86*, 404.

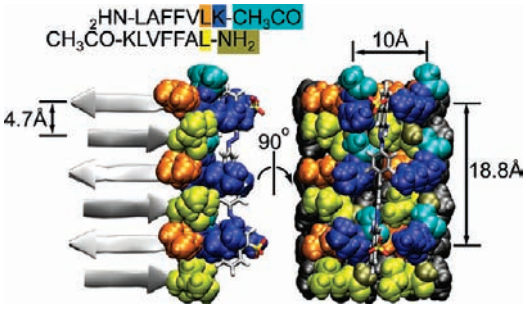


***Figure 6.*** Model of the CR-KLVFFAL laminate groove site. The residues in close proximity to CR are shown in space-filling format as follows: $CH_3CO$ N-terminal capping group (cyan), Lys-16 (blue), Leu-17 (orange), Phe-19 (gray), and Phe-20 (gray), Leu-22 (yellow), and the $-NH_2$ C-terminal capping groups (brown). Congo Red is displayed in stick format with C (gray), O (red), N (blue), H (white), and S (yellow).

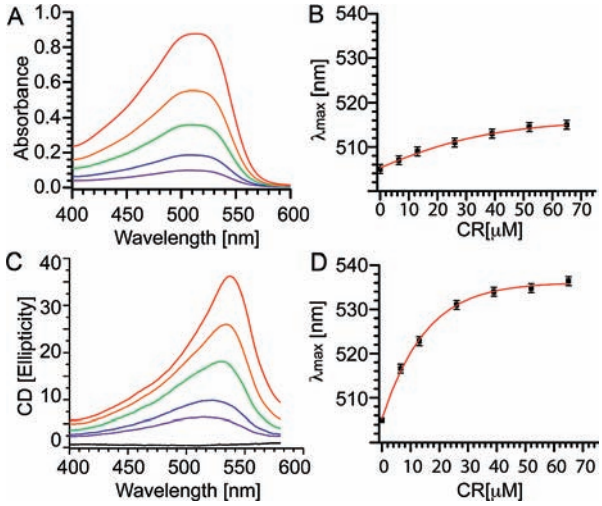


***Figure 7.*** (A) UV/vis and (C) CD spectra at different KLVFFAL:CR ratios with KLVFFAL peptide nanotubes assembled from 650 $\mu$M KLVFFAL peptide: black (65 $\mu$M CR only), violet (100:1), blue (75:1), green (50:1), orange (20:1), and red (10:1). (B) Plots of UV/vis $\lambda_{max}$ and (D) CD $\lambda_{max}$ as a function of CR concentration.

molecules were manually docked along the laminate grooves and energy minimized with implicit water (Figure 6). In the resulting models, CR spans ~6 peptides (5 × 4.7 Å) along the laminate groove, consistent with the 6.1 ± 0.5 peptide:CR binding ratio calculated above and earlier charge-directed models.[16] Charge complementarity between the negatively charged CR sulfates and positively charged lysine side-chains was easily maintained in these models.

**CR Binds at High Density.** To test for CR−CR interactions, UV−vis/CD spectra were collected at various peptide:CR ratios. A concentration-dependent red-shift is seen in both UV−vis absorption and CD spectra (Figure 7). However, induced-CD reports only on molecules bound to amyloid, and both the red-shift and the change in CD band shape are consistent with coupled oscillator interactions between neighboring CR electronic transition dipoles.

Indeed, exciton coupling theory[49,50] predicts a red-shift in $\lambda_{max}$ of chromophores with electronic transition dipoles oriented

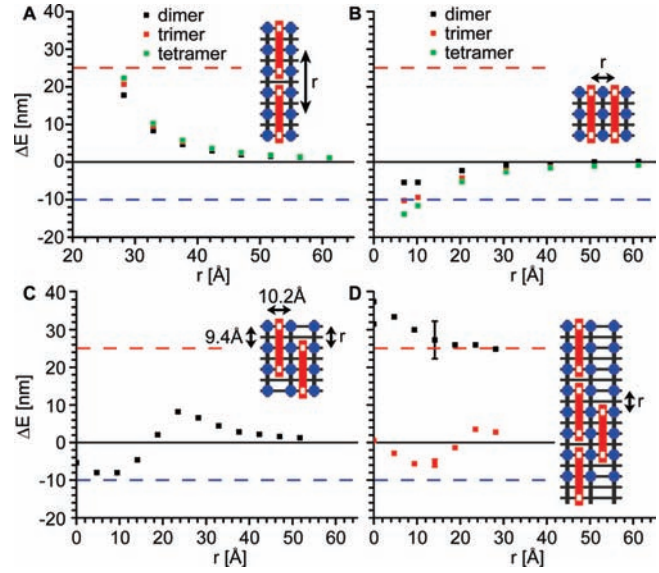


***Figure 8.*** Calculated ZINDO/S exciton coupling energy ($\Delta E$) of (A) CR end-to-end or J-aggregates and (B) CR side-to-side or H-aggregates as a function of center-to-center distance. In (C), CR registry within H-aggregates is evaluated, and in (D), the registry of a monomer relative to a J-aggregate CR trimer is evaluated. The red and blue dashed horizontal lines represent the observed red- and blue-shifts for bound CR (Figure 2C). The inset cartoons display laminate grooves with $\beta$-sheets separated by 10.2 Å and H-bonded peptides by 4.7 Å. The blue circles represent N-terminal lysines and the white squares the CR sulfates. $\Delta E$ is the energy splitting arising from exciton coupling and is the difference in transition frequency between the aggregate and monomer. In Figure 8D, we have assigned the red-shifted transition (black squares) to J-aggregation, and the blue-shifted transition (red squares) is predominantly due to the H-like aggregate. The error bars represent the expected range in exciton coupling arising from variations in binding geometry, calculated by moving the single molecule in the adjacent laminate and the middle molecule in the laminate with three CR molecules by 1 Å in all directions.

end-to-end as J-aggregates and a blue-shift for transition dipoles organized side-by-side as H-aggregates. Quantum chemical calculations were employed to investigate the observed 25 nm red-shift and 10 nm blue-shift of $\lambda_{max}$ in the observed UV−vis spectra. As the magnitude of the coupling between the individual CR electronic transition dipoles, hence the effect on the UV−vis spectra, depends on both the number of molecules and their relative orientations, the calculations must be performed on several molecules. Because of the relatively large number of atoms in CR, calculating the vertical electronic transitions at the 6-31G+(d,p) level of theory proved to be computationally impractical for systems with more than a single CR molecule. However, semiempirical quantum-chemical (ZINDO/S[43,44]) methods have been shown to be a good compromise between accuracy and computational cost for predicting the effects on electronic transitions resulting from the interaction of molecules within an aggregate.[51−53]

The results for CR J-aggregates confirmed the red-shifted J- (Figure 8A) and blue-shifted H- (Figure 8B) aggregate predictions. As expected, the calculated shift in $\lambda_{max}$ increases as the center-to-center distance is decreased, but even the closest spacing expected for only two CR molecules bound to the

(49) Kasha, M. *Rev. Mod. Phys.* **1959**, *31*, 162.
(50) Harada, N. N.; Nakanishi, K. *Circular Dichroic Spectroscopy. Exciton Coupling in Organic Stereochemistry*; University Science Books: Mill Valley, CA, 1983.
(51) Wichard, J. D. B.; Tonu, P. *J. Chem. Phys.* **2004**, *120*, 2490.
(52) Beljonne, D.; Cornil, J.; Silbey, R.; Millie, P.; Bredas, J. L. *J. Chem. Phys.* **2000**, *112*, 4749.
(53) Howard, I. A.; Zutterman, F.; Deroover, G.; Lamoen, D.; Van Alsenoy, C. *J. Phys. Chem. B* **2004**, *108*, 19155.

cross-$\beta$ laminate grooves does not match the experimentally observed shifts (horizontal red and blue lines in Figure 8A/B). However, the coupling strength ($\Delta E$) for trimer and tetramer CR systems increases, suggesting that the trimeric and tetrameric CR systems contain enough molecules to accurately reproduce the CR aggregate arranged on the cross-$\beta$ laminate surface. Fixing CR molecules to neighboring laminates (Figure 8C) reveals the orientation dependence of the exciton coupling. The pure H-character becomes more J-like as the center-to-center distance between the molecules is increased. Saturated binding is approximated in Figure 8D. The resulting ZINDO calculations for the systems with both J- and H-aggregate character show both red- and blue-shifted electronic transitions (Figure S1). Even though saturated binding is approximated with only 4 CR molecules, the calculated magnitude of the exciton coupling for the J band is on the order of that observed in the UV−vis absorption spectra. The underestimate of the H-band blue-shift mostly likely arises from only having an H-aggregate dimer. To test the influence of the helical nature of the amyloid nanotube surface on the CR spectroscopic signature, a planar tetramer was compared to a helical tetramer (Figure S4), and little difference was found.

## Discussion

The common link among all amyloid diseases and infectious prions is amyloid deposition. CR staining[1,16,41] has proven to be a robust diagnostic for these structures, regardless of primary sequence. The amyloid nanotube morphology uniquely reduces the complexity of the amyloid surface and allows direct interrogation of CR binding to cross-$\beta$ laminate grooves. Bound CR displays the hallmark signatures of amyloid: apple-green interference color[1,41] and a red-shifted 505 nm transition.[16] The peptide:CR binding ratio (6.1 ± 0.5) for amyloid nanotubes is the same as the binding ratios previously indicated for A$\beta$(1−40).[16] However, others[29] have reported more saturated CR binding stoichiometery to A$\beta$(1−40), with ratios near 1:1, which may indicate additional binding modes.

Initial investigations with ab initio[19] and ZINDO/S (Figure 1A, iii) calculations place the lowest energy transition dipole moment of CR parallel to the long axis for both cis and trans conformations of the heterocyclic dye. Linear dichroism measurements place the long axis of CR offset 0−14° from the nanotube axis and collinear with $\beta$-sheet laminate grooves, which maintain a 13 ± 2° offset from the amyloid long-axis. The resulting periodic cross-$\beta$ arrangement of peptides forms an amphiphilic surface capable of positioning several CR molecules in close proximity (<10 Å). Such proximity positions CR molecules well within the range of distance-dependent exciton coupling for both J-aggregates (<45 Å, Figure 8A) and H-aggregates (<30 Å, Figure 8B).

The calculated exciton coupling ($\Delta E$) for a Jelly−Scheibe (J)-aggregate[54,55] of a CR tetramer separated by a center-to-center distance of 28.2 Å is 23 nm, consistent with the 25 nm red-shift observed for CR bound to the A$\beta$(16−22) amyloid illustrated in Figure 9B. However, the frequency range observed in the UV−vis absorption spectra is broad (dashed line in Figure 9), extending below the monomer $\lambda_{max}$ at 505 nm. This broadening is distinct from the calculated transition for the isolated J-aggregate (Figure 9B) and the sharp J-band observed in other systems.[56,57] Similarly, the laminate cross-$\beta$ structure,

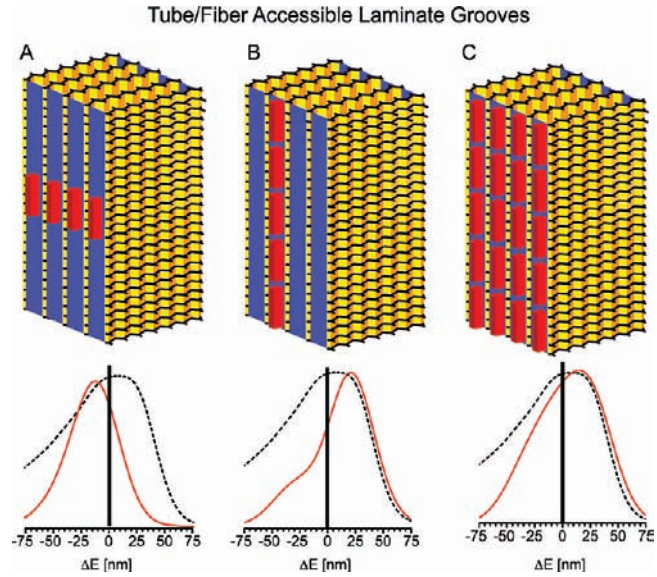


***Figure 9.*** Simulated UV−vis of different CR packing arrangements on the laminate groove surface. (A) Isolated H-aggregate tetramer, (B) J-aggregate tetramer, and (C) saturated laminate groove. $\Delta E$ is the energy shift arising from exciton coupling and is the difference in transition frequency between the aggregate and monomer. The solid curve is the calculated UV−vis spectrum, and the dashed line is the experimental UV−vis absorption for a peptide:CR ratio of 10:1. The saturated laminate groove (C) was approximated as in Figure 8D.

which arranges CR side-by-side as H-aggregates, separated by multiples of 10.2 Å, should display only a blue-shift (Figure 9A). The combined contribution of CR J-aggregates and H-aggregates is supported by intensity increases at both 495 and 530 nm (Figure 9C). Shifts in registry could result in a slight red-shift, and, therefore, the position of the H-band may well report on the registry of CR bound in neighboring grooves. Although an offset H-aggregate registry of 14.1 Å (Figure 8D) best fits the experimental data and is consistent with charge complementation, both variations in splitting observed when the molecules are displaced by only 1 Å, and the restricted size of the computation currently makes this assignment tenuous. Furthermore, a Hill plot coefficient of 1.2 ± 0.2 is consistent with noncooperative binding up to a peptide:CR ratio of 6:1.

Figure 10 summarizes the overall structural model, highlighting the central hydrophobic residues, LVFFAL in gray, and the positively charged lysine residues at the $\beta$-sheet ends in blue. The laminate groove therefore consists of walls of lysine residues above a floor covered by the hydrophobic L22 and L17 side-chains. Because of the antiparallel nature of the $\beta$-sheet,[34] the lysine α-carbon to α-carbon spacing is 9.4 Å along the $\beta$-sheet and 10.2 Å between sheets. The position of CR docked within these grooves matches the sulfate negative charge distance, 19 Å with 5 hydrogen-bonded peptides (4 × 4.7 Å). The next CR molecule within a laminate, docked at the available lysine, sets the center-to-center CR distance to 28 Å (6 × 4.7 Å). As the distance between the inner and outer tube walls is 40 Å,[35] binding to the inner and outer tube surfaces will create H-aggregate dimers that are separated by 40 Å, consistent with a very small (<1 nm) blue-shift.

(54) Jelley, E. E. *Nature* **1936**, *138*, 1009.
(55) Scheibe, G.; Rivas, A. *Angew. Chem., Int. Ed. Engl.* **1936**, *49*, 0443.
(56) Ohno, O.; Kaizu, Y.; Kobayashi, H. *J. Chem. Phys.* **1993**, *99*, 4128.
(57) Harrison, W. J.; Mateer, D. L.; Tiddy, G. J. T. *J. Phys. Chem.* **1996**, *100*, 2310.

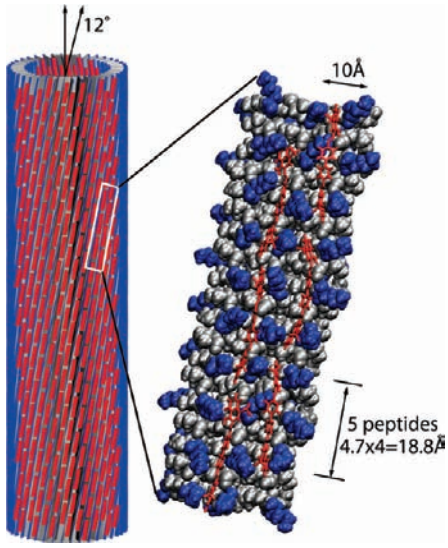


***Figure 10.*** Model of amyloid nanotubes saturated with CR.

A conformational change extending CR conjugation has been proposed to result in a red-shift[58] as illustrated in Figure S6. However, the gradual red-shift in $\lambda_{max}$ observed in the CD binding saturation experiment (Figure 7B/D) is inconsistent with a single optically active conformation. It is possible that a population of CR conformations gives rise to the observed red- and blue-shifts; however, Hill plot analysis indicates noncooperative binding upon saturation. To account for changes in the observed $\lambda_{max}$, the population of multiple conformations would have to change as binding sites become saturated, and each conformation has roughly the same binding affinity. Here, we propose a simpler CR−CR exciton coupling model to account for spectral shift changes. The ZINDO calculations of vertical electronic transitions for various CR organizations (Figure S5) highlight why this dye is so universally diagnostic. Binding parallel to the fiber axis[59] results in well-defined and densely packed J-aggregates. Relative shifts of the J-aggregates in adjacent binding grooves or within a groove will have only subtle effects on the observed UV of bound CR. Additionally, due to the planar nature of CR, the transition dipole of the molecule is roughly independent of biphenyl conformation.[19] The red-shift observed in the UV−vis absorption difference spectrum of bound and unbound CR[4,16] will be dominated by the J-band. These characteristics allow CR to be a robust, universal identifier of amyloid's periodic cross-$\beta$ arrays.

The CR templated assembly presented here is consistent with the polarizing microscopy results acquired on several amyloid plaques[59] and the pioneering work[60,61] indicating that all amyloids bind Congo Red in a common mode parallel to the $\beta$-sheet axis. This model is consistent with previous proposals in which CR interacts with the peptide termini parallel to the fiber axis as illustrated in Figure 1A, i.[16] However, there may well be other binding modes open for CR and other ligands. For example, it has been proposed that Thioflavin T (ThT) binds within the $\beta$-sheet pleat grooves.[30,62−64] Preliminary results (data not shown) indicate ThT has very weak affinity for A$\beta$(16−22) laminate grooves, consistent with ThT and CR having different binding sites.[29] Smaller amyloid ligands (i.e., FDDNP and ThT derivatives)[29] may preferentially target the smaller $\beta$-pleat surfaces over the larger laminate grooves.

The periodic cross-$\beta$ arrays of both nanotubes and traditional amyloid fibers have the capacity to template arrays of CR in close proximity where exciton coupling effects may be observed. Helical cross-$\beta$ nanotubes and typical twisted amyloid fibrils differ predominantly with access to the pleat surface (yellow surfaces in Figures 1 and 9). This pleat surface could harbor additional ligand binding sites that are inaccessible in nanotubes. If these pleats in amyloid fibers become saturated, CR molecules would be templated as arrays separated by ~7 Å, as opposed to ~10 Å, resulting in a more blue-shifted H-band (ZINDO/S calculations indicate a 2 nm larger shift going from the CR tetramer with a 10 to a 7 Å spacing, Figure 8B). In contrast, the laminate grooves investigated here are common to both cross-$\beta$ nanotubes and fibers. The primary difference is the number of parallel laminate grooves: 3−6 for fibers and greater than 100 for nanotubes, which could result in a larger H-aggregate for nanotubes relative to fibers. As well, the side-chain composition within the laminate grooves from different amyloid structures varies dramatically, which could modulate relative binding affinities. The pH dependence of CR binding to a variety of A$\beta$(1−40) truncations indicates that histidine residues can influence CR binding and suggests a CR binding motif of His13−His14−Gln15−Lys16.[9] Interestingly, the most highly resolved structural model of A$\beta$(1−40) amyloid fibers[13,14] places His13 along the laminate grooves.

Previously, we have shown that extension of the A$\beta$(16−22) peptide to HAQKLVFFA forms toxic amyloid fibers and templates the assembly of copper ions into linear arrays separated by 9.4 Å within its laminate groove.[65] It may well be that amyloid's ability to precisely organize entities, ranging from metal ions[65,66] to CR, lies at the heart of its functional significance. Sequestering specific metabolites at precise positions within amyloid's cross-$\beta$ grooves from the cytosol could have a profound impact on neurons. Indeed, recent studies of amyloid's role in the melanosome[8] have suggested such functional interactions. With this foundational insight into amyloid's molecular templating capability, the variations in primary sequence and higher order structural folds (bends, loops, and disordered regions) localized within laminate and pleat grooves can now be exploited as diagnostic fingerprints[67] of amyloid strains and highlight differences that distinguish "toxic", "functional", and "nontoxic" amyloid.

**Acknowledgment.** We are indebted to Jeannette Taylor and the Robert P. Apkarian Microscopy Core, Emory University, for

(58) Miura, T.; Yamamiya, C.; Sasaki, M.; Suzuki, K.; Takeuchi, H. *J. Raman Spectrosc.* **2002**, *33*, 530.
(59) Jin, L.-W.; Claborn, K. A.; Kurimoto, M.; Geday, M. A.; Maezawa, I.; Sohraby, F.; Estrada, M.; Kaminksy, W.; Kahr, B. *Proc. Natl. Acad. Sci. U.S.A.* **2003**, *100*, 15294.
(60) Taylor, D. L.; Allen, R. D.; Benditt, E. P. *J. Histochem. Cytochem.* **1974**, *22*, 1105.
(61) Benditt, E. P.; Eriksen, N.; Berglund, C. *Proc. Natl. Acad. Sci. U.S.A.* **1970**, *66*, 1044.
(62) Krebs, M. R. H.; Bromley, E. H. C.; Donald, A. M. *J. Struct. Biol.* **2005**, *149*, 30.
(63) Wu, C.; Wang, Z. X.; Lei, H. X.; Duan, Y.; Bowers, M. T.; Shea, J. E. *J. Mol. Biol.* **2008**, *384*, 718.
(64) Biancalana, M.; Makabe, K.; Koide, A.; Koide, S. *J. Mol. Biol.* **2009**, *385*, 1052.
(65) Dong, J.; Canfield, J. M.; Mehta, A. K.; Shokes, J. E.; Tian, B.; Childers, W. S.; Simmons, J. A.; Mao, Z.; Scott, R. A.; Warncke, K.; Lynn, D. G. *Proc. Natl. Acad. Sci. U.S.A.* **2007**, *104*, 13313.
(66) Dong, J.; Shokes, J. E.; Scott, R. A.; Lynn, D. G. *J. Am. Chem. Soc.* **2006**, *128*, 3540.
(67) Ashburn, T. T.; Han, H.; McGuinness, B. F.; Lansbury, P. T. *Chem. Biol.* **1996**, *3*, 351.

training and collection of TEM and electron diffraction. We also thank Prof. Dev Arya of Clemson University for access to LD and Dr. Jamal Musaev in the Emerson Computational Center for advice on quantum calculations and the NSF (CHE-0131013) for CD instrumentation. This work was funded by the U.S. DOE (ER15377), NSF (CRC-CHE-0404677), and NSF-CBC-0739189. We also thank Prof. Dale Edmondson and Stefan Lutz for advice during the course of this research.

**Supporting Information Available:** TEM images of KLVFFAL nanotubes with and without CR; calculated ZINDO spectra of helical versus planar CR tetramers, and for various CR arrangements within laminate grooves; and calculated CR $\lambda_{max}$ as a function biphenyl conformation. This material is available free of charge via the Internet at http://pubs.acs.org.

JA902332S